Gaussian core model in two dimensions. I. Melting transition

Frank H. Stillinger and Thomas A. Weber

Bell Laboratories, Murray Hill, New Jersey 07974
(Received 20 November 1980; accepted 12 December 1980)

The method of molecular dynamics computer simulation has been used to examine the solid–fluid transition for the Gaussian core model in two dimensions. The system contained 780 particles subject to periodic boundary conditions, and confined to a single reduced density $\rho^* = 3^{-1/2}$. The virial pressure, mean potential energy, and pair correlation functions all indicate that the melting process is first order. However, the system is anomalous in that thermal expansivities of the solid and (low temperature) fluid phases are negative, and the density change on melting at constant pressure is positive.

I. INTRODUCTION

Recent experimental and theoretical developments have created substantial interest in two-dimensional solid–fluid transitions. On the one hand, it has been possible to produce such transitions in the laboratory with electrons on the liquid helium surface,[1] with free films of smectic liquid crystals,[2] and with polystyrene spheres at the air–water interface.[3] On the other hand, theory has suggested that under some circumstances the transformation from solid to isotropic fluid could occur by a pair of continuous transitions, into, and then out of an intervening "hexatic" phase.[4,5]

As a result of these activities, desire has been heightened to establish definitively the melting transition behavior of selected two-dimensional theoretical models. Specific cases thus far examined include the rigid disk system,[6] the family of models with simple inverse power pair potentials,[7–10] and the two-dimensional Lennard-Jones system.[10–13] The first of these appears to undergo a conventional first-order melting. Conflicting evidence has been presented on whether the latter types can yield hexatic phases, or whether only the normal first-order melting process obtains.

In addition to resolving uncertainties over the behavior of those specific models it remains of interest to expand the set of models (i.e., potentials) that have been quantitatively examined and understood. It is for this latter reason that we have studied the two-dimensional version of the classical Gaussian core model[14] by means of molecular dynamics computer simulation. Although this model contains the rigid disk system as a special limiting case, it nevertheless displays unusual features not shared by the other models mentioned. One of these features is a "volume" (i.e., area) of melting that varies continuously from positive to negative as the system is compressed. Due to the difficulty of generating accurate, complete, and reproducible results in the melting transition region we have been forced to limit our present investigation to a single density, but it is one for which the unusual thermal behavior is well developed (negative melting area, negative thermal expansion in both fluid and solid phases).

The following (Sec. II) reviews the basic properties of the Gaussian core model. This is followed in Sec. III by a brief statement of the molecular dynamics procedure employed. Section IV presents results both for thermodynamic properties and for molecular distribution functions. Section V summarizes our conclusions.

A companion paper[15] provides a detailed analysis of topological order in the various states of the two-dimensional Gaussian core model using nearest neighbor polygons.

II. GAUSSIAN CORE MODEL

The Gaussian core model is defined by its potential energy function Φ. For N particles Φ takes the following simple form in reduced length and energy units that are natural to the problem:

$$\Phi = \sum_{i<j=1}^{N} \exp(-r_{ij}^2) \,. \tag{2.1}$$

As a result of the repulsions between particles, the lowest energy configuration for large N will be crystalline. In three dimensions the ordered phase is face-centered cubic at low density and body-centered cubic at high density.[14] In two dimensions a detailed study of lattice sums reveals the expected result, namely that the triangular (close-packed) lattice yields the absolute minimum for Φ at all densities.

In order to produce the rigid disk model from the Gaussian core system it is necessary simultaneously to go to low temperature *and* low density.[14] Let $F_G^{(ex)}(\beta, \rho)$ be the excess Helmholtz free energy for N Gaussian particles at inverse temperature β and number density ρ, and let $F_{RD}^{(ex)}(\beta, \rho)$ be the same quantity for N disks with diameter a. Then we have

$$\lim_{\beta\to\infty} \frac{F_G^{(ex)}(\beta, \rho_0 a^2/\ln\beta)}{F_{RD}^{(ex)}(\beta, \rho_0)} = 1 \,, \tag{2.2}$$

provided that the disk density does not exceed close packing, i.e.,

$$\rho_0 a^2 < 2/\sqrt{3} \,. \tag{2.3}$$

Regardless of the spatial dimension D, the Gaussian core model possesses a duality relation that links pairs of zero-temperature lattice sums at high and at low density.[16] If we write

$$I = \lim_{N\to\infty} (2\Phi/N) + 1 \tag{2.4}$$

for twice the potential energy per particle of the ordered array (including a self-energy term + 1) in the infinite

 0021-9606/81/074015-05$01.00

system limit, then

$$(\rho_h^*)^{-1/2} I(\rho_h^*) = (\rho_l^*)^{-1/2} I(\rho_l^*) , \tag{2.5}$$

where the high and low reduced densities ρ_h^* and ρ_l^* are related by

$$\rho_h^* \rho_l^* = \pi^{-D} . \tag{2.6}$$

This density duality stems simply from the fact that the Gaussian function is self-similar under Fourier transformation.

Beside possessing a duality relation, the Gaussian core model is analytically pleasing in that the logarithm of its partition function can be developed readily in a high temperature expansion. Explicit coefficients (as functions of ρ and D) are now available for this series through eighth order.[17]

III. SIMULATION PROCEDURE

Our molecular dynamics simulation has employed $N = 780$ particles confined to a rectangular unit cell whose area is such that the reduced density has the fixed value

$$\rho^* = 3^{-1/2} . \tag{3.1}$$

This falls in the high-density regime, since ρ^* exceeds the fixed-point value π^{-1} for the duality relation at $D = 2$.

The shape of the unit cell was chosen so that with periodic boundary conditions imposed, a perfect and aligned 26×30 crystal just fits in its interior. Under this circumstance the cell is nearly square; the ratio of its sides is precisely

$$15\sqrt{3}/26 = 0.999\,260\ldots . \tag{3.2}$$

Because the Gaussian pair potential declines toward zero so rapidly with increasing distance it is possible to carry out the simulation virtually without a cutoff on interactions. In fact, we have actually disregarded interactions between particles so far apart that

$$\exp(-r_{ij})^2 < \exp(-28) = 7 \times 10^{-13} . \tag{3.3}$$

This criterion as well as the integration algorithm and time step for the dynamical equations remain unchanged from our earlier three-dimensional studies with the Gaussian core model.[18–20]

For most of the thermodynamic states examined, dynamical runs of 13 000 steps were employed. The first 1000 were disregarded to eliminate equilibration transients, while the remainder were broken into three equal segments of 4000 steps with separate averages that could be intercompared for statistical significance.

IV. RESULTS

A. Pressure

We have used the two-dimensional version of the virial theorem to evaluate the pressure. Figure 1 exhibits the results for reduced pressure p^* versus reduced temperature T^*.

In the low temperature regime, where the stable phase is the triangular lattice, two close, nearly parallel, but

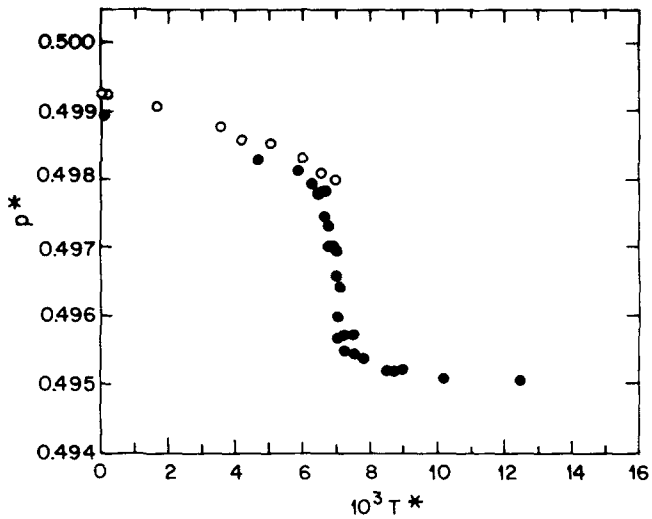

FIG. 1. Reduced pressure p^* versus reduced temperature T^* for the two-dimensional Gaussian core model at reduced density $\rho^* = 3^{-1/2}$. Open circles at low T^* refer to a perfect and aligned lattice, while solid circles in the same range refer to a misoriented crystal containing a pair of interstitials.

distinguishable branches are shown. One of these (open circles) corresponds to a perfect crystal that is free of defects and aligned with the sides of the unit cell. Our calculations were initiated with this ideal structure at very low temperature, and then successive temperature jumps were imposed to approach the melting point. The other branch (solid circles) was generated subsequently by spontaneous freezing upon slow cooling of the high temperature fluid. The crystal that formed in this latter case was misoriented with respect to the sides of the unit cell (by approximately 14°) and in its ideal form would contain precisely 778 particles. The two excess particles produced by the fact that $N = 780$ then appeared as a pair of highly mobile interstitials whose presence was obvious when computer-drawn pictures of the instantaneous configuration were produced. Of the two branches shown for the crystal we believe that the former (open circles, no defects) is more indicative of the true thermodynamic behavior below the melting point.

The most striking attributes of the results in Fig. 1 are that (a) the pressure declines with increasing temperature throughout the solid phase region; (b) there is a sudden drop in pressure in the range

$$T_m^* = 6.6 \times 10^{-3} \leq T^* \leq T_f^* = 7.2 \times 10^{-3} \tag{4.1}$$

(which our monitoring of particle mobility identifies as the melting range) indicative of a first-order transition with a negative melting area; and (c) the negative temperature coefficient of pressure continues beyond the melting range [Eq. (4.1)] into the pure fluid phase. The pressure, in fact, appears to pass through a very flat minimum around $T^* = 1.2 \times 10^{-2}$. It is interesting that each of these features also occurs in the three-dimensional version of the model at high density.

The observation that the pressure for the imperfect crystal is less than that for the perfect version is con-

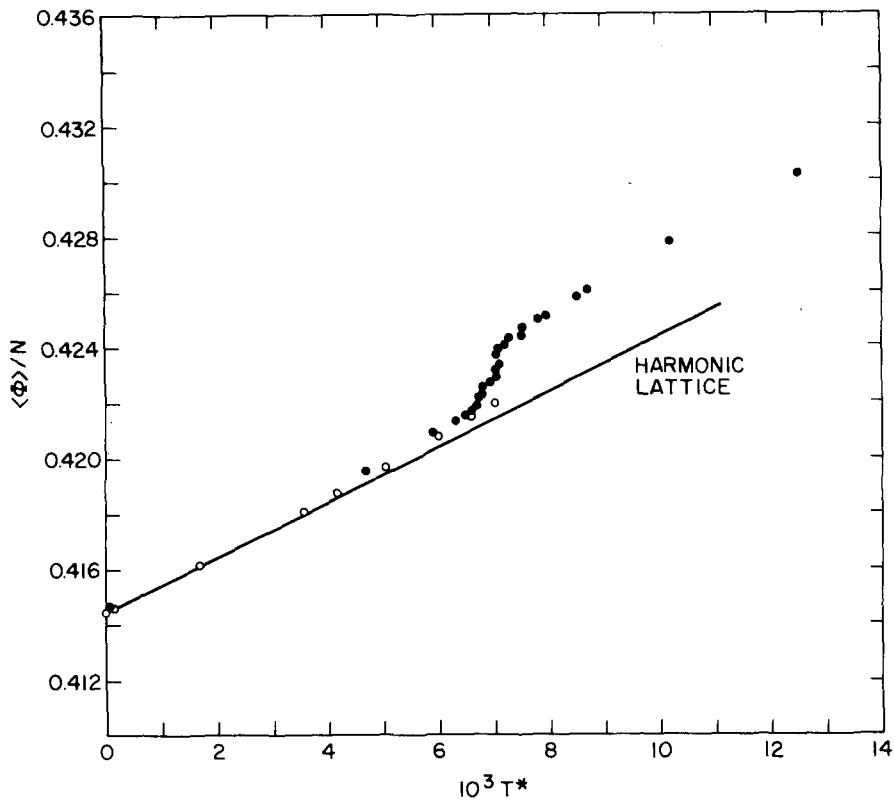

FIG. 2. Mean potential energy per particle $\langle\Phi\rangle/N$ versus reduced temperature T^*. As in Fig. 1 the open and closed circles at low temperature refer to the perfect and imperfect crystals, respectively.

sistent with the fact that melting (a major insertion of imperfection) also reduces pressure.

The perfect crystal tends easily to superheat since it has no obvious sites for nucleation. In this respect it is advantageous to utilize a slightly imperfect crystal to determine the melting temperature T_m^*. We found that the two-interstitial case represented in Fig. 1, upon subsequent slow reheating through the melting interval [Eq. (4.1)], retraced essentially the same $p^*(T^*)$ it exhibited on cooling. This absence of hysteresis in the melting range gives us confidence that T_m^* and T_f^* have been correctly identified.

Taking due account of the finite system size (which tends to "round" transitions), it appears that the pressure results indicate that a first-order melting exists at the given density. In this connection it is worth pointing out that states near the middle of the melting range have indefinite lifetimes as such. They do not fluctuate in pressure alternately between values identifiable as extensions of solid and of fluid phase branches, respectively. Instead, intermediate pressure values occur as would be expected for coexisting solid and fluid. This presumption of the achievability of long-lived coexistence is confirmed by analysis of nearest-neighbor polygon patterns in the following paper.[15]

B. Average potential energy

Figure 2 presents our results for $\langle\Phi\rangle/N$, the mean potential energy per particle. As before, the perfect and imperfect crystal results below T_m^* are shown separately. By extrapolation to absolute zero we find that the potential energy difference between these two structures is

$$\Delta\Phi = 0.168\,05\ . \tag{4.2}$$

Once again, the pattern shown in Fig. 2 is characteristic of a simple first-order melting process. Within the previously identified melting range the slope of the implied $\langle\Phi\rangle/N$ curve is anomalously large compared to that of the neighboring pure phases, due to absorption of a latent heat. If the melting process were carried out at a fixed pressure equal to that shown in Fig. 1 for the midpoint of the transition range

$$p^* = 0.4967\ , \tag{4.3}$$

we estimate that the corresponding latent heat would be

$$\Delta H/N = 0.0021\ . \tag{4.4}$$

Upon dividing by the temperature at this midpoint ($T^* = 6.9\times10^{-3}$) we conclude that the transition entropy must be

$$\Delta S/Nk_B = 0.30 \pm 0.01\ . \tag{4.5}$$

This is comparable to other entropies that have been observed for two-dimensional melting transitions with soft-core particles,[10] though possibly it is somewhat smaller than that for rigid disks.[6,10]

The harmonic crystal result, a straight line, has been inserted in Fig. 2 for comparison, with intercept chosen to agree with that for the perfect crystal. Although it is obvious that the Gaussian core model behaves harmonically at low temperature (whether the structure is that of a perfect crystal or not), it is also obvious that anharmonicity intrudes as T^* approaches T_m^* from below. The tendency for the slope in Fig. 2 to exceed that of the harmonic crystal, i.e., for the constant-density heat capacity to increase, is typical for very soft interactions.

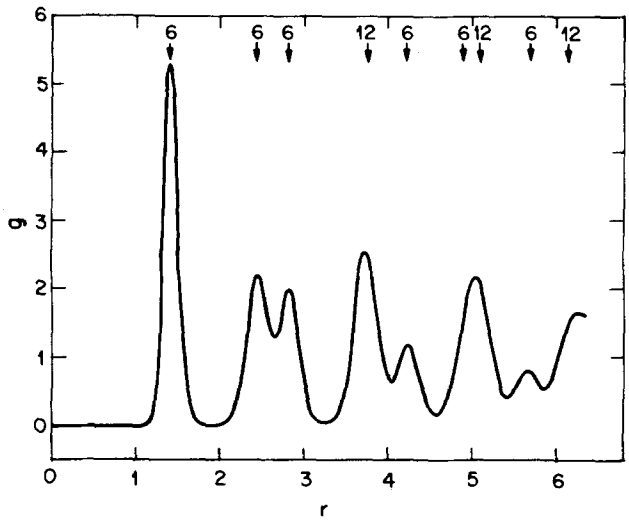

FIG. 3. Pair correlation function for the perfect crystal at $T^* = 3.56 \times 10^{-3}$. Positions and numbers of neighbors for the thermally unexcited crystal are indicated at the top.

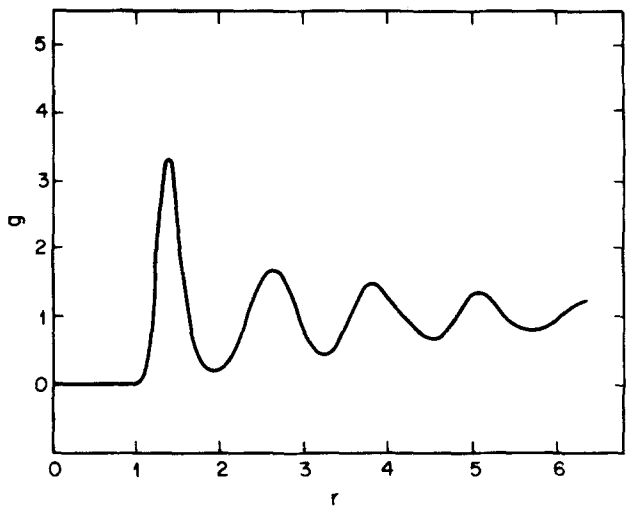

FIG. 5. Pair correlation function at $T^* = 7.01 \times 10^{-3}$, midway across the transition range.

C. Pair correlation function

The distribution of particle pair separations conveyed by the pair correlation function $g(r)$ is a sensitive quantitative indicator of local structure. In a closed finite system, such as the one we have used, this function is defined such that the angle-averaged probability that a distinct pair of differential area elements $d\mathbf{r}_1$ and $d\mathbf{r}_2$ in the system simultaneously host particles is

$$N(N-1)\,g(r_{12})\,d\mathbf{r}_1\,d\mathbf{r}_2\,/A^2\ . \tag{4.6}$$

Here, A stands for the system area.

At low temperature the successive coordination shells of the triangular lattice stand out vividly in $g(r)$. Figure 3 shows this behavior for the perfect crystal at reduced temperature 3.56×10^{-3}, or approximately half the melting temperature. The $g(r)$ for the imperfect crystal looks very similar to that for the perfect case at the same temperature, though with slightly less distinct maxima and minima.

Figures 4, 5, and 6 show how the pair correlation changes as the system is slowly cooled through the transition range so it spontaneously freezes. The first of these, Fig. 4, shows the result obtained for the homogeneous fluid at $T^* = 7.24 \times 10^{-3}$, just barely above T_f^*. Subsequent cooling caused nucleation of the crystal to occur. Figure 5 displays $g(r)$ at $T^* = 7.01 \times 10^{-3}$, approximately midway across the transition region. Further cooling caused the freezing to complete (into the defective crystal, as explained above). Figure 6 shows $g(r)$ in the fully frozen state at $T^* = 6.46 \times 10^{-3}$.

The structural evolution in the system upon passing reversibly across the transition region is clearly conveyed by Figs. 4, 5, and 6. Obviously, the maxima

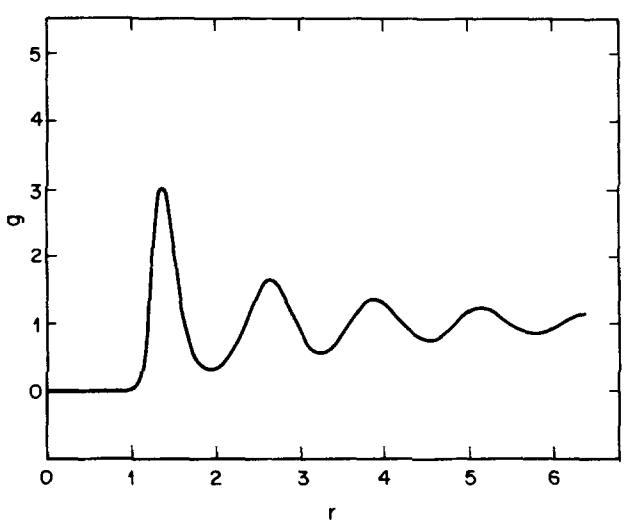

FIG. 4. Pair correlation function for the homogeneous fluid at $T^* = 7.24 \times 10^{-3}$, just above the freezing point.

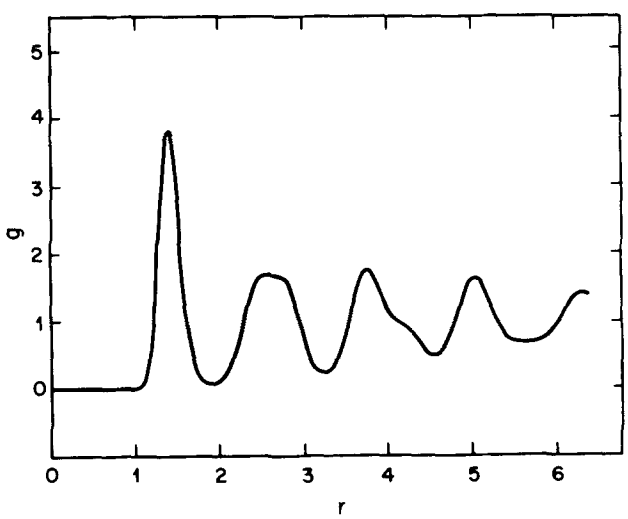

FIG. 6. Pair correlation function at $T^* = 6.46 \times 10^{-3}$, just below the melting temperature. The crystal structure formed by spontaneous freezing is slightly imperfect, as explained in the text.

and minima in $g(r)$ become better developed as a result of freezing; the value of g at its first maximum changes from 3.05 in Fig. 4, to 3.31 in Fig. 5 and to 3.79 in Fig. 6. But, at the same time the regular damped oscillations that appear in the fluid-phase function are replaced by less symmetric maxima and minima that stem from the peculiar distribution of coordination shell radii in the triangular lattice. Close inspection reveals that the $g(r)$ peaks in Fig. 6 are just thermally broadened versions of those shown in Fig. 3 for the crystal at lower temperature.

That $g(r)$ in Fig. 5 is intermediate between those of Fig. 4 (fluid) and Fig. 5 (crystal) is consistent with phase coexistence.[21]

V. CONCLUSIONS

The results presented above seem consistently to indicate that at $\rho^* = 3^{-1/2}$ the melting transition occurs in a conventional first-order manner, rather than via a pair of higher-order transitions into and out of an orientationally (but not translationally) ordered hexatic phase.[4,5] Further details supplied by the topological analysis of nearest neighbor polygons in the following paper[15] strengthen this conclusion. Of course, we cannot at present exclude the possibility that the hexatic phase would appear at some other density.

In view of the fact that the Gaussian core model continuously approaches the rigid disk case at low density, and since rigid disks likewise appear not to exhibit hexatic-phase melting, it seems to us unlikely that the fundamental melting mechanism will change through the range $0 < \rho^* < 3^{-1/2}$. The only novelty expected within this range is the existence of a point at which the melting density changes sign (from positive at $\rho^* = 3^{-1/2}$ to negative in the rigid disk limit). Thermodynamics requires that the melting and freezing temperature $T_m^*(\rho^*)$ and $T_f^*(\rho^*)$ achieve a common maximum at this point.

Consequently, any future search for the hexatic phase in the Gaussian core system should be directed toward $\rho^* > 3^{-1/2}$. Application of the duality relations[16] shows that all lattice packings of Gaussian core particles asymptotically approach a common energy as ρ^* increases, suggesting that the melting point converges to zero in this limit, so simulations would have to be carried out with scrupulous attention paid to matters of precision, equilibration, and reproducibility. By examining phonon spectra for the model we have discovered that in the same large-ρ^* limit the crystal becomes exceptionally soft to transverse phonons, particularly near the midpoints of the boundaries of the hexagonal Brillouin zone. It will be interesting to see if this softening substantially influences the melting process.

[1] C. C. Grimes and G. Adams, Phys. Rev. Lett. 42, 795 (1979).
[2] D. E. Moncton and R. Pindak, Phys. Rev. Lett. 43, 701 (1979).
[3] R. Pieranski, Phys. Rev. Lett. 45, 569 (1980).
[4] B. I. Halperin and D. R. Nelson, Phys. Rev. Lett. 41, 121 (1978); 41, 519 (1978).
[5] D. R. Nelson and B. I. Halperin, Phys. Rev. B 19, 2457 (1979).
[6] B. J. Alder and T. E. Wainwright, Phys. Rev. 127, 359 (1962).
[7] R. W. Hockney and T. R. Brown, J. Phys. C 8, 1813 (1975).
[8] R. C. Gann, S. Chakravarty, and G. V. Chester, Phys. Rev. B 20, 326 (1979).
[9] R. H. Morf, Phys. Rev. Lett. 43, 931 (1979).
[10] F. van Swol, L. V. Woodcock, and J. N. Cape, J. Chem. Phys. 73, 913 (1980).
[11] D. Frenkel and J. P. McTague, Phys. Rev. Lett. 42, 1632 (1979).
[12] F. F. Abraham, Phys. Rev. Lett. 44, 463 (1980).
[13] S. Toxvaerd, Phys. Rev. Lett. 44, 1002 (1980).
[14] F. H. Stillinger, J. Chem. Phys. 65, 3968 (1976).
[15] T. A. Weber and F. H. Stillinger, J. Chem. Phys. 74, 4020 (1981) (following paper).
[16] F. H. Stillinger, Phys. Rev. B 20, 299 (1979).
[17] F. H. Stillinger, J. Chem. Phys. 70, 4067 (1979).
[18] F. H. Stillinger and T. A. Weber, J. Chem. Phys. 68, 3837 (1978); 70, 1074 (1979).
[19] F. H. Stillinger and T. A. Weber, J. Chem. Phys. 70, 4879 (1979).
[20] F. H. Stillinger and T. A. Weber, Phys. Rev. B 22, 3790 (1980).
[21] J. E. Mayer and E. Montroll, J. Chem. Phys. 9, 2 (1941).